THE ASTROPHYSICAL JOURNAL, 419:658–669, 1993 December 20

THE POPULATION OF MASSIVE STARS IN R136 FROM FAINT OBJECT CAMERA ULTRAVIOLET OBSERVATIONS[1]

GUIDO DE MARCHI,[2,3] ANTONELLA NOTA,[2,4] CLAUS LEITHERER,[2] ROBERTO RAGAZZONI,[5] AND CESARE BARBIERI[6]
Received 1993 February 23; accepted 1993 June 28

ABSTRACT

New ultraviolet ($\lambda \simeq 1300$ Å, $\lambda \simeq 3400$ Å), *HST* Faint Object Camera observations have been used to derive the UV color-magnitude diagram (CMD) of R136. The main scientific goal is the study of the upper end of the stellar mass function at ultraviolet wavelengths where the color degeneracy encountered in visual CMDs is less severe.

The CMD has been compared to a set of theoretical isochrones, which have been computed using the latest generation of evolutionary models and model atmospheres for early-type stars. Wolf-Rayet stars are included, and their emergent fluxes are calculated with the theoretical continuum energy distributions of Schmutz et al. Comparison of the *theoretical* and *observed* CMD suggests that there are no stars brighter than $M_{130} \simeq -11$.

We use the observed main sequence turnoff and the known spectroscopic properties of the stellar population to derive constraints on the most probable age of R136. The presence of WNL stars and the lack of red supergiants suggests a most likely age of 3 ± 1 Myr. A theoretical isochrone of 3 ± 1 Myr is consistent with the observed stellar content of R136 if the most massive stars have initial masses around $\simeq 50\ M_{\odot}$.

Subject headings: Hertzsprung-Russell diagram — Magellanic Clouds — open clusters and associations: individual (R136) — ultraviolet: stars

1. INTRODUCTION

R136 is the brightest cluster in the giant H II region 30 Doradus in the Large Magellanic Cloud. R136a is its bright core, which remained unresolved for many years. The interpretation of the nature and the stellar content of R136a has been controversial. Once it was believed to be a single superluminous object (Feitzinger et al. 1980; Cassinelli, Mathis, & Savage 1981). From ultraviolet observations, Savage et al. (1983) suggested that the radiation from R136 was dominated by emission from a single supermassive star ($\simeq 2100\ M_{\odot}$) or a small group of supermassive stars whose formation would have occurred by ordinary stellar collapse in a region containing peculiar dust or by the coalescence of stars in a region of high star density.

Later Worley (1984) used astrometric observations over a time span of 58 years to conclude that R136a was a nebulous double with a position angle approximately 220°. Other, slightly more distant components had already been observed by van den Bos (1928).

The first speckle interferometry observations (Meaburn et al. 1982) failed to detect any form of multiplicity, but were later proved inaccurate by other speckle observers (Weigelt & Baier 1985; Neri & Grewing 1988) who confirmed, albeit with some disagreement about the detailed structure, that R136a was indeed a cluster, composed of several unresolved sources.

These results were also supported by the high resolution observation made with the fast tip-tilt seeing corrector by Maaswinkel et al. (1988). However, only several years later the *Hubble Space Telescope* (*HST*) unambiguously resolved and measured the flux of the brightest components, both with the Faint Object Camera (FOC) (Weigelt et al. 1991) and with the Wide Field Planetary Camera (Campbell et al. 1992; Malumuth & Heap 1992).

R136a itself is resolved into at least 12 components (Campbell et al. 1992), three of which are found to be Wolf-Rayet (W-R) stars from the emission in the He II λ4686 line. The brightest stars within R136 are found to have luminosities and colors of *normal* massive stars still on the main sequence or already evolved into the supergiant or Wolf-Rayet phases—in contrast to other more massive stars observed elsewhere in 30 Doradus. This is in overall agreement with the claim of Moffat, Seggewiss, & Shara (1985), and previously Moffat & Seggewiss (1983) who had already suspected, from ground-based aperture spectrophotometry, that R136 *does not* contain extraordinarily bright stars.

The age of the R136 cluster and its history of star formation is still argument of debate (Lortet & Testor 1991): the original prevailing idea was that 30 Doradus is a very young structure energized mainly by R136. Following the discovery of an older population of stars (McGregor & Hyland 1981), a two-burst-type star formation was suggested. Later Walborn (1986) and Melnick (1987) attributed the existence of a wide spread of ages in the region to a continuous, nonviolent star formation process across the entire nebula. Lortet & Testor (1991) relate this continuous range in ages of stars to the morphology of the neighboring gas. Ages seems to increase with distance from the center of R136. Moffat et al. (1987) compared the W-R population at different ranges of distances from R136 across the whole LMC. Walborn (1986) showed that stars in the immediate surroundings of R136 ($r < 30''$) are younger than more distant ones. However, with the discovery of other very early-

[1] Based on observations with the NASA/ESA *Hubble Space Telescope*, obtained at the Space Telescope Science Institute, which is operated by AURA, Inc., under NASA contract NAS5-26555.

[2] Space Telescope Science Institute, 3700 San Martin Drive, Baltimore, MD 21218.

[3] On leave from Dipartimento di Astronomia, Università di Firenze, Italy.

[4] Affiliated with the Astrophysics Division, Space Science Department of the European Space Agency.

[5] Osservatorio Astronomico di Padova, Vicolo Osservatorio 5, 35122 Padova, Italy.

[6] Dipartimento di Astronomia, Università di Padova, Vicolo Osservatorio 5, 35122 Padova, Italy.

type stars and an H_2O maser at several arcminutes from R136, no distinct separation can be made between stars of different ages in contrast to what has been found in the case of less massive H II regions such as N158 in the LMC (Lortet & Testor 1988).

In this paper we present a discussion of new results we have obtained on the stellar content, age, and evolutionary state of the very nucleus of 30 Doradus using *HST* FOC images taken in the UV. The unambiguous advantage of investigating in the far-UV bandpasses is to resolve of the color degeneracy which affects visual color-magnitude diagrams (CMDs) and allows us to characterize in detail the properties of the most massive objects present in the core of the cluster.

2. OBSERVATIONS AND DATA REDUCTION

Observations of R136 were performed on 1990 August 22, 1991 January 4, and 1991 February 2 with the FOC in its F/96 mode. The FOC camera characteristics are described in detail in Paresce (1992) and Greenfield et al. (1991). The 1990 August 22 observation, taken as part of the early scientific assessment period, was obtained with the filter combination F346M + F8ND, and an exposure time of 597 s. A few months later, four additional images of the same region were taken for calibration purposes with the filter F130M and an exposure time of 900 s each. The exposures were taken in a sequence with subsequent offsets of 5″in α and δ to cover a larger area of 32″ × 32″ with partial overlap. In Table 1 we list characteristics and exposure times of this image set.

The two filters used, F130M and F346M, have peak transmission at 1280 and 3450 Å, respectively, with a bandpass of 88 Å (FWHM) for the F130M and of 432 Å for the F346M.

The camera format consistently adopted for all these exposures has 512 × 1024 pixels, producing a total field of view on the sky of 22″ × 22″. In the geometrical corrected image, the pixels are rectangular, 0″.44 × 0″.22 in size. As a result of the pipeline dezooming algorithm, each rectangular pixel is split into two square pixels of 0″.22 × 0″.22, each containing half the flux of the original rectangular pixel. This large camera format has a limited dynamic range (8 bits pixel^{-1}): as a consequence, even if the source count rate is well within the linear regime of the FOC, the brightest pixels can be affected by numerical wrap-around effects. This limitation, however, can be satisfactorily overcome and the photometric accuracy restored, as we will discuss later on.

The point-spread function (PSF) in our images has a FWHM core of 4.6 pixels for both filters, and the encircled energy in the core is approximately 11% of the total flux. Due to the *HST* primary mirror spherical aberration, the remaining light is distributed over a circular halo of radius about 2″ (Burrows et al. 1991).

The raw frames have been flat-fielded to correct the pixel-to-pixel nonuniformities and then geometrically corrected in order to remove distortions due to the detector and the optical system. The three deepest out of the four F130M images, largely overlapping, have been used to create a single, high signal-to-noise image of the central area of the cluster. Accurate registration of the frames was achieved by two independent methods: first, rectangular coordinates of selected stars were determined in each frame, and the average shift and rotation angle were calculated and used to achieve a good alignment of the fields of view. Second, we cross-correlated all possible image pairs, both in Cartesian and polar coordinates. The $(x\text{-}y)$ and (ρ, θ) location of the main peak of the cross-correlation function gave the amount of the shift needed to exactly register our images (Barbieri, De Marchi, & Ragazzoni 1991). Both methods agreed on the registration parameters to within 0.5 pixel. This result has been confirmed by a further check which consisted of measuring the FWHM of the stars in the summed image in comparison to the stars in the initial images. The two measures agreed to better than 0.5 pixel.

Our four images are well within the linear regime of the FOC but, as already mentioned, they are affected by numerical wrap-around, due to the limited dynamic range of the 8 bit camera format used. Numerical wrap-around effects occur every time the number of counts in a generic pixel exceeds 256. Consequently, the counter is reset to zero, and this shows in the image as a zero intensity hole in the brightness peak. The wrap-around affects only the pixels in which this condition is verified, but these pixels do not necessarily correspond to the peaks of the brightest stars, because the limit can be reached even by a fainter star sitting on the halo of a brighter object. Fifty-nine stars in the F130M frames are affected by wrap-around. Forunately, the fourth F130M frame (listed in Table 1 as exposure 5) lasted only half the scheduled exposure time, resulting in a numerically corrected image for all the stars but one. Frame 5 has been used to recover the true peak counts of the 59 "wrap-arounded" stars by fitting a suitably scaled PSF to their wings. After this correction, the overall internal error on the photometry of these stars is estimated not to exceed approximately 0.05 mag.

The final summed F130M image is shown in Figure 1 (Plates 3–4). The F346M image has been aligned to the F130M sum by using the same registration technique. The resulting overlap area of the two filters is ~ 113 arcsec^2, but the two images differ considerably in quality: using the brightest stars we can estimate that the S/N ratio in the F130M summed image is ~ 28, while it is ~ 7 in the F346M frame. The S/N is calculated in both cases from photon statistics, in the central pixel.

TABLE 1

OBSERVATION LOG OF THE FOC FRAMES

Number	Frame Number	Exposure Date	Exposure Time (s)	Filter
1.....	X0BQ0101T	1990 Aug 23	597	F346M + F8ND
2.....	X0FC0202T	1991 Jan 5	897	F130M
3.....	X0FC0203T	1991 Jan 5	897	F130M
4.....	X0FC0207T	1991 Jan 5	897	F130M
5.....	X0GC0101T	1991 Feb 3	402	F130M

3. THE PHOTOMETRY

The first step in the photometric reduction procedure consists in the location of the peak of each star in the F130M image, using DAOPHOT (Stetson 1987). The same set of coordinates is then used as a first guess to identify the stars in the F346M image, which has a lower signal-to-noise ratio, and then to derive their final positions in the frame.

In order to distinguish true and spurious detections due to features in the PSF tendrils, an objective criterion is imposed to retain as "true" only stars with a S/N ratio of at least 2.5 in the peak, resulting in the location of 221 stars common to both frames.

The photometric reduction is carried out following the technique called *core aperture photometry* (Gilmozzi 1990; Paresce et al. 1991). The technique consists of first computing the stellar flux in a very small aperture of radius slightly smaller than the full width at half-maximum (FWHM) of the PSF.

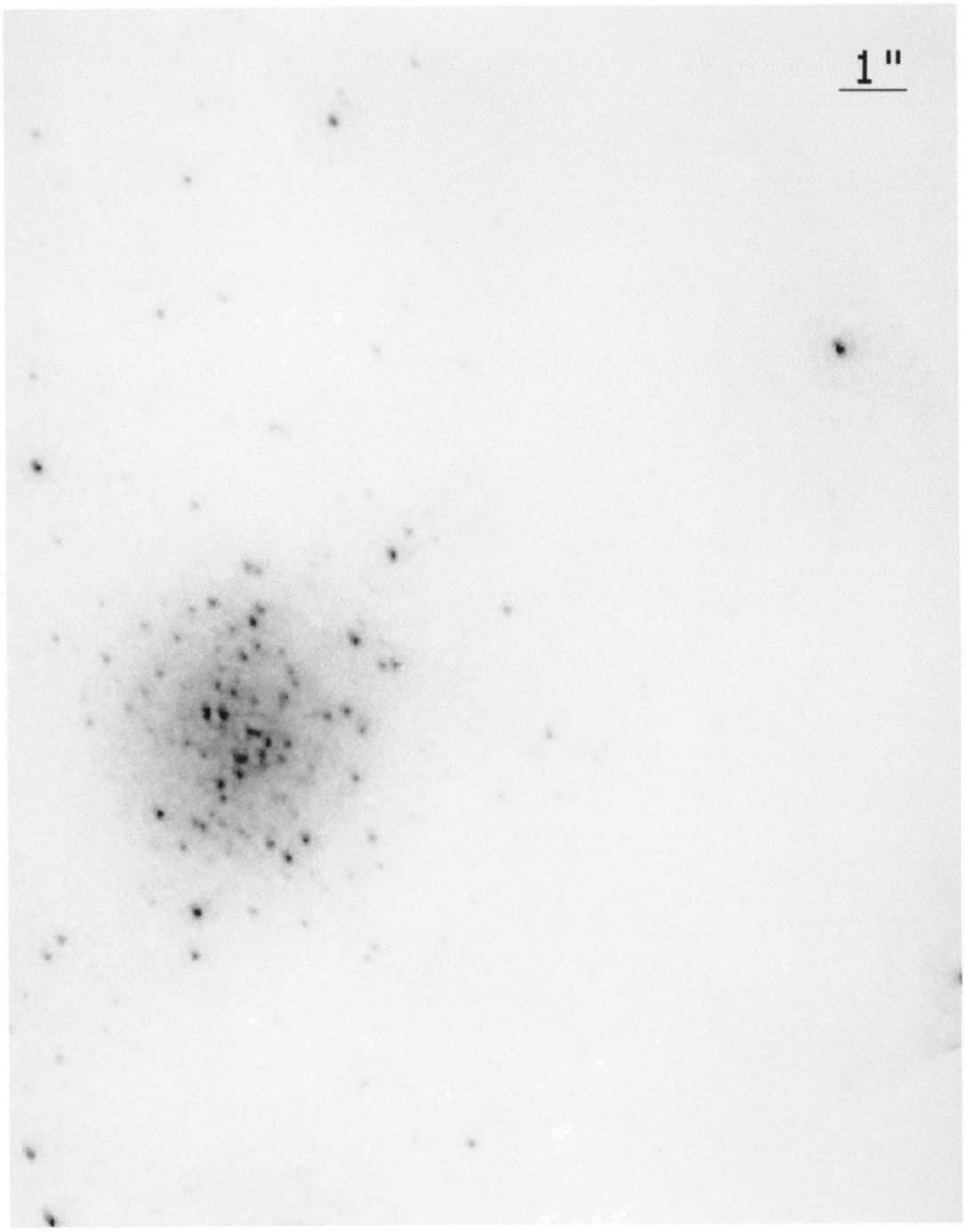

FIG. 1*a*

FIG. 1.—(*a*) Final summed F130M image. Area of the image is $\simeq 113$ arcsec^2, with a scale of 0.″022 pixel^{-1}. North is up and East to the left. (*b*) Enlargement of the 4.″4 × 4.″4 region around the cluster center (derived with a mirror autocorrelation technique). Weigelt's components R136a_1-a_8 have been labeled.

DE MARCHI et al. (see 419, 659)

PLATE 4

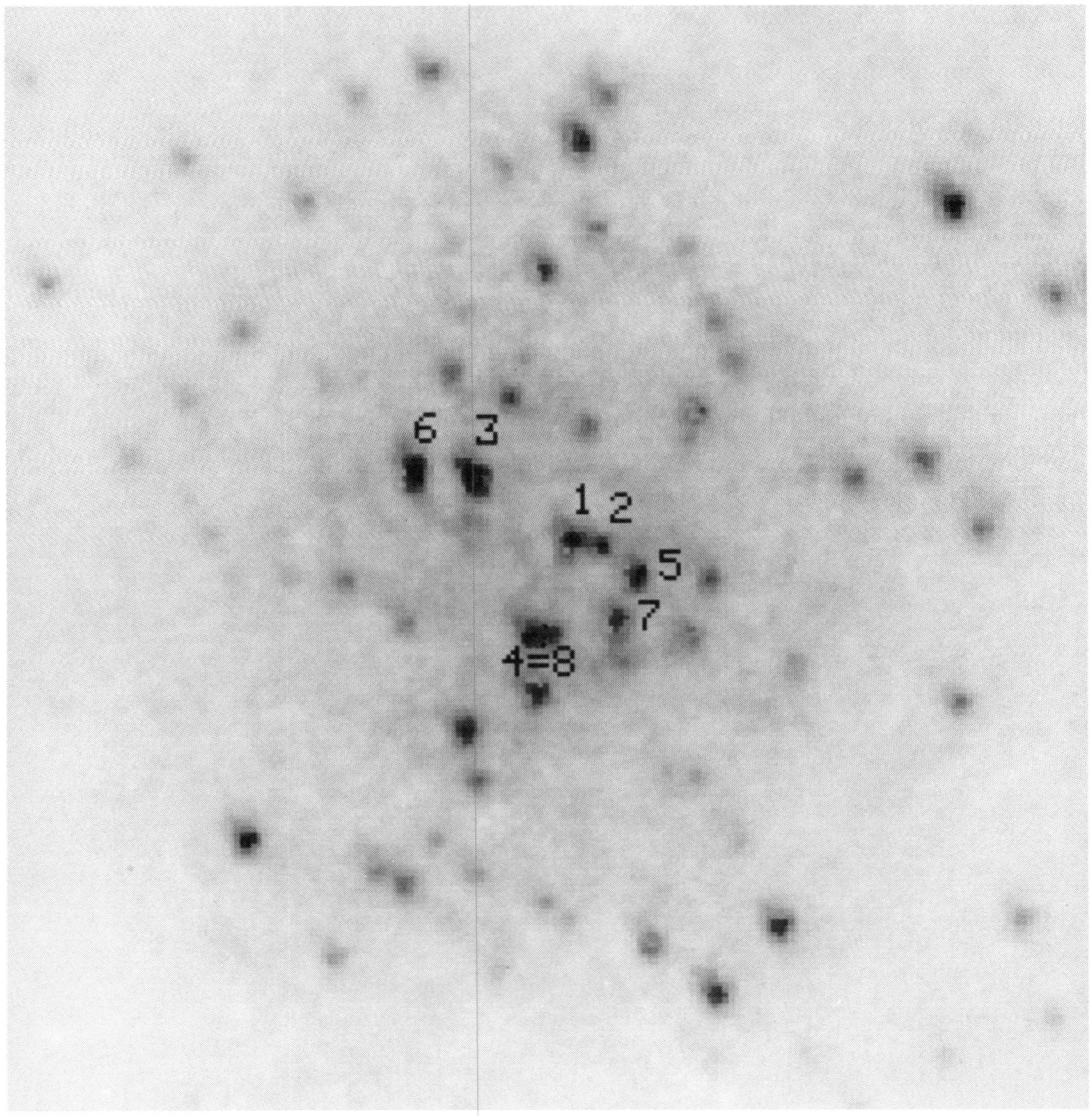

FIG. 1*b*

DE MARCHI et al. (see 419, 659)

Then the background is measured by taking the mode (instead of the mean) of an annulus centered on each star peak, with the external radius well within the PSF halo. The advantage of selecting the background very close to the central star peak is twofold: it is possible to do accurate photometry of a very crowded field *and* in the presence of a spatially variable background. However, due to the spherical aberration, a significant fraction of the source light is distributed in the halo and contaminates the background measurement. In order to perform the background subtraction correctly it is therefore necessary to estimate the fraction of source light present in the background annulus. In other words, it is necessary to know how the PSF encircled energy (defined as flux percentage contained in the area at a given radius) varies as a function of the distance from the peak. We have measured the encircled energy as a function of the radial distance from the center for a number of isolated standard photometric stars. Those data were taken with the same two filters approximately at the same time and telescope focus setting of our observations, and correction factors for both wavelengths have been determined.

Aperture photometry has then been performed. On the F130M image, a core radius of 4 pixels, corresponding to $\simeq 0''.088$ (approximately the FWHM of the PSF) and an annulus with internal and external radius of 6 ($\simeq 0''.132$) and 8 pixels ($\simeq 0''.176$) for the background, respectively, has been used. Due to the different shape of the PSF on the F346M image, the radius is 2 pixels ($\simeq 0''.044$) for the core aperture and the background annulus is chosen between 4 ($\simeq 0''.088$) and 6 pixels ($\simeq 0''.132$). The resulting fluxes have been corrected to include the encircled energy correction factors previously derived.

It is crucial to understand that the overall accuracy of the photometry is critically sensitive to the choice of the core radius and background distance. Reasons include the variable shape of the PSF as a function of wavelength, the intrinsic structural differences between the PSFs in the two filters, and the crowding of the cluster area. As we are working on geometric corrected images, the PSF remains constant across the field, so we can neglect any positional effect. Several tests have been made in which we varied the two parameters. We estimate a relative photometric error of approximately 0.05 mag for the brightest objects, but slowly degrading with magnitude, for our choice of core radius and background distance.

We generated monochromatic magnitudes m from the fluxes in the filter bandpasses using the relation given in the FOC Handbook (Paresce 1992), and revised in the UV response from in-flight calibration data (Sparks 1991):

$$m = -21.10 - 2.5 \log \left[\frac{(F-B) \times U}{\epsilon \times t} \right]. \quad (1)$$

F is the number of counts falling within the core aperture; B is the background value, estimated for each single object as already explained; U is the inverse sensitivity of the instrument mode (camera + filters); ϵ is the encircled energy falling within the core aperture; and t is the total exposure time. In our case we have $U_{130} = 1.584 \times 10^{-15}$ ergs cm^{-2} Å^{-1}, $U_{346} = 5.89 \times 10^{-18}$ ergs cm^{-2} Å^{-1} (taking into account that the F346M exposure was taken through a neutral density filter F8ND); $t_{130} = 3093$ s while $t_{346} = 597$ s. We estimate an accuracy of approximately 20% on the absolute photometry due to the high uncertainty associated to the FOC absolute photometric calibration in the UV.

The data are presented in Table 2, where column (1) gives our internal identification number, columns (2) and (3) give the coordinates of the detected stars, and columns (4) and (5) the F130M and F346M magnitudes, respectively (m_{130}, m_{346}). The coordinates of the stars are given with respect to a rectangular grid whose axes are aligned to the S and L axes of the detector as described in the *FOC Handbook*, and are expressed in unit of pixels (1 pixel = $0''.022$). The eight R136 components originally identified by Weigelt & Baier (1985) are flagged in the table. We note that Weigelt's stars a_4 and a_8 are indeed the same object, numbered 185 in our list.

4. INTERSTELLAR EXTINCTION IN R136

We have computed the absolute magnitudes M_{130}, M_{346} from the apparent magnitudes presented in Table 2, adopting a distance module of 18.55 ± 0.13 (Panagia et al. 1991). These have been corrected for interstellar extinction. A large uncertainty is associated with the extinction law in the UV (Ardeberg 1976; Braunsfurth & Feitzinger 1983; Moffat et al. 1987; Lortet & Testor 1991). This is mainly due to the lack of comprehensive data on the absorption and reddening intrinsic to the cluster, and to the fact that even small errors in the visible region translate into large errors in the UV. As discussed by Fitzpatrick & Savage (1984), the total intervening absorption is due to three contributions, the Milky Way (MW), the LMC foreground in the 30 Doradus region (LMC), and the 30 Doradus nebular dust (ND).

For the first component, there is general consensus (e.g., Brunet 1975; Isserstedt 1975) that

$$E(B-V)^{\rm MW} = 0.07 \quad \text{and} \quad R_V^{\rm MW} = 3.1 \rightarrow A_V^{\rm MW} = 0.22 . \quad (2)$$

The standard MW UV absorption curve (Fitzpatrick 1985) provides $A_{346}^{\rm MW} = 0.36$, $A_{130}^{\rm MW} = 0.64$ and therefore $(A_{130} - A_{346})^{\rm MW} = 0.28$.

An ample range of values for $E(B-V)$, A_V and R_V can be found in the literature for the second contribution. We adopted Fitzpatrick's (1985) method, which has been derived for LMC objects:

$$E(B-V)^{\rm LMC} = 0.16 \quad \text{and} \quad R_V = 3.1 \rightarrow A_V^{\rm LMC} = 0.50 . \quad (3)$$

Using the LMC UV absorption curve for the region of 30 Doradus (Fitzpatrick 1985) we obtain $A_{346}^{\rm LMC} = 0.82$, $A_{130}^{\rm LMC} = 2.10$ so that $(A_{130} - A_{346})^{\rm LMC} = 1.28$.

Following Fitzpatrick & Savage (1984) we adopt

$$E(B-V)^{\rm ND} = 0.18 \quad \text{and} \quad R_V = 3.7 \rightarrow A_V^{\rm ND} = 0.67 \quad (4)$$

for the third contribution. Since the UV curve for this nebular dust component is flatter than both the LMC intrinsic and the Milky Way extinction curve (Fitzpatrick & Savage 1984), the absorption coefficients become $A_{346}^{\rm ND} = 1.03$, $A_{130}^{\rm ND} = 1.57$, and $(A_{130} - A_{346})^{\rm ND} = 0.54$. As we will discuss in more detail later on, the LMC absorption due to both the stellar and dust components is highly variable and position dependent across the region. The available information, derived for selected areas of the 30 Doradus nebula will be used as a first iterative guess for our isochrone fitting.

Summarizing, the adopted values are:

$$E(B-V) = 0.41$$
$$A_V = 1.39$$
$$A_{346} = 2.21$$
$$A_{130} = 4.31$$
$$(A_{130} - A_{346}) = 2.10 .$$

TABLE 2

STELLAR PHOTOMETRY OF R136

ID	X	Y	m_{130}	m_{346}	ID	X	Y	m_{130}	m_{346}	ID	X	Y	m_{130}	m_{346}
1	56	8	15.4	16.3	61	216	270	15.2	16.4	121	84	390	15.7	16.6
2	108	15	15.0	15.8	62	117	274	15.3	14.5	122	210	394	16.8	17.0
3	54	20	16.6	16.4	63	144	275	14.4	15.4	123	98	397	14.0	15.0
4	153	28	15.9	15.5	64	171	274	15.3	15.5	124	243	400	14.6	15.6
5	29	32	16.9	16.3	65	200	275	14.1	15.0	125	223	403	16.2	16.1
6	10	33	15.7	16.4	66	280	275	15.1	15.9	126	273	403	16.0	16.0
7	306	36	15.9	15.1	67	142	277	15.2	15.5	127	154	406	15.0	15.5
8	205	40	15.2	15.3	68	170	281	15.3	16.5	128	130	408	14.1	14.7
9	320	60	13.5	14.3	69	115	281	15.4	15.6	129	246	408	15.5	15.0
10	282	63	15.4	15.3	70	338	289	14.8	14.9	130	190	408	15.6	15.4
11	21	95	15.2	15.7	71	376	289	15.3	14.7	131	218	409	16.3	16.9
12	48	96	15.9	16.6	72	239	293	15.0	15.9	132	341	409	13.5	13.8
13	249	100	14.9	15.9	73	137	295	14.9	15.3	133	69	412	14.7	15.5
14	44	114	14.2	14.8	74	75	299	15.6	16.7	134	100	411	16.1	16.8
15	97	120	15.8	16.3	75	93	299	14.8	16.2	135	112	412	16.2	15.7
16	395	121	15.7	15.9	76	204	298	14.8	15.6	136	225	412	17.0	15.5
17	10	133	14.4	15.9	77	302	304	16.4	15.8	137	191	421	15.6	15.6
18	74	133	15.0	15.3	78	235	305	15.6	15.9	138	252	422	15.7	16.5
19	323	136	15.9	16.0	79	210	306	14.3	15.7	139	271	423	16.3	17.4
20	190	140	15.2	15.6	80	401	314	15.3	15.8	140	162	425	16.2	16.7
21	81	152	14.9	15.1	81	87	315	16.5	15.0	141	173	433	13.6	14.4
22	20	156	14.7	15.7	82	284	318	15.9	16.4	142	211	437	15.0	15.9
23	191	172	16.0	15.9	83	361	319	15.8	15.4	143	221	444	15.6	15.6
24	249	182	14.5	14.7	84	216	319	14.9	15.2	144	276	445	14.9	14.4
25	140	188	15.5	15.3	85	195	322	13.6	14.0	145	39	452	14.5	15.5
26	254	189	14.4	14.9	86	226	321	16.5	15.8	146	293	455	14.9	15.3
27	44	192	13.6	14.7	87	117	323	14.6	15.3	147	274	460	13.9	13.9
28	301	193	15.3	15.4	88	208	323	15.9	16.1	148	286	472	16.1	15.8
29	197	202	16.9	16.2	89	370	329	13.9	14.2	149	131	476	14.0	15.3
30	129	204	15.0	16.3	90	254	330	14.9	15.4	150	227	479	15.8	15.9
31	207	204	14.4	14.6	91	151	332	13.9	14.9	151	298	481	15.5	16.1
32	173	211	14.0	14.6	92	62	334	14.1	15.2	152	248	484	14.9	15.2
33	30	215	16.0	16.3	93	228	336	15.0	16.5	153	84	494	14.8	15.3
34	142	216	14.1	14.8	94	98	336	15.7	15.4	154	192	524	14.8	16.0
35	105	218	14.8	15.3	95	253	336	14.9	14.7	155	183	527	14.2	14.6
36	240	217	15.7	15.6	96	207	340	16.6	17.5	156	154	533	15.9	15.3
37	123	222	17.5	17.1	97	214	341	14.5	15.6	157	97	540	15.3	15.5
38	221	227	14.8	15.6	98	73	353	16.1	15.4	158	22	559	14.0	15.3
39	99	227	15.2	16.0	99	280	352	16.4	15.6	159	83	592	15.8	15.4
40	18	230	15.9	16.3	100	99	354	14.3	15.0	160	107	601	13.6	14.7
41	119	231	15.9	16.1	101	209	357	16.9	17.6	161	149	611	14.3	15.6
42	140	235	17.6	15.6	102	125	357	15.2	16.0	162	28	645	15.5	16.3
43	196	235	14.6	15.8	103	130	358	16.2	16.9	163[a6]	141	341	12.2	12.8
44	238	235	15.1	15.3	104	249	357	16.9	15.9	164	191	312	13.5	14.7
45	104	240	17.3	15.8	105	306	359	16.1	15.2	165	175	381	14.3	14.6
46	165	242	15.7	15.6	106	81	360	15.0	15.9	166	40	6	12.1	12.8
47	257	242	14.6	15.3	107	144	363	14.3	15.5	167	25	51	12.9	14.5
48	13	246	15.2	16.1	108	207	363	14.9	15.0	168	35	181	13.5	14.8
49	179	248	15.5	16.7	109	247	369	16.0	16.0	169	134	182	13.2	14.0
50	196	247	12.6	13.8	110	295	372	15.6	15.9	170	135	210	12.2	13.1
51	156	252	14.4	15.5	111	122	379	16.1	16.3	171	125	254	14.0	14.8
52	108	255	16.0	16.0	112	52	383	15.4	15.5	172	184	256	13.1	13.9
53	216	255	14.8	15.1	113	190	380	13.7	14.6	173	207	259	12.8	13.9
54	92	257	16.5	17.0	114	78	381	15.5	15.8	174	164	263	14.5	15.2
55	168	260	14.0	14.9	115	50	384	15.6	15.4	175	138	267	13.2	14.5
56	147	261	15.7	17.0	116	84	387	16.2	17.0	176	151	269	14.2	14.8
57	252	260	13.7	14.1	117	257	387	14.8	15.7	177	109	275	12.6	13.4
58	185	265	14.5	15.6	118	38	388	14.2	15.3	178	152	285	13.4	14.8
59	103	269	16.9	15.5	119	193	388	14.8	15.3	179	192	286	14.0	14.6
60	182	268	15.8	15.4	120	120	389	13.8	14.6	180	150	294	12.6	13.7

TABLE 2—*Continued*

ID	X	Y	m_{130}	m_{346}	ID	X	Y	m_{130}	m_{346}	ID	X	Y	m_{130}	m_{346}
181	240	299	13.3	14.1	195	185	335	14.5	14.8	209	258	372	13.3	13.8
182	163	301	12.8	14.1	196	178	339	15.8	14.7	210	266	373	13.1	14.1
183	151	305	14.7	15.2	197	221	339	13.2	13.9	211	73	375	14.0	14.6
184	178	308	13.3	14.5	198[a3]	151	340	12.1	12.3	212	165	377	13.1	13.7
185[a4,a8]	162	312	12.7	13.2	199	158	341	13.8	13.2	213	174	384	13.5	14.0
186	139	314	13.8	14.1	200	234	343	13.2	13.8	214	240	388	12.4	12.6
187[a7]	178	314	12.8	13.3	201	172	349	14.0	15.0	215	157	395	14.0	14.8
188	128	321	13.5	14.2	202	192	351	13.2	13.8	216	171	400	12.6	13.5
189[a5]	181	322	12.8	13.3	203	158	354	13.4	14.1	217	176	408	13.2	13.7
190	160	327	14.7	15.6	204	147	358	13.2	14.8	218	144	413	13.3	14.4
191[a2]	174	328	12.5	12.2	205	199	360	13.6	14.8	219	167	436	13.5	14.4
192[a1]	170	328	12.6	11.8	206	160	361	13.7	14.8	220	264	445	12.5	12.5
193	187	327	14.4	14.6	207	109	366	13.8	15.0	221	25	500	12.5	13.2
194	245	331	13.2	13.9	208	196	368	13.4	14.5					

This is our preferred estimate for total intervening absorption and reddening. The derived magnitudes have been corrected with these absorption values. We notice here, however, that if we adopted the MW UV absorption curve as representative also of the LMC stellar and dust components, we would have found $A_V = 1.29$, $A_{346} = 2.11$, and $A_{130} = 3.75$, implying $(A_{130} - A_{346}) = 1.64$, and our absolute color-magnitude diagram would have been ~ 0.5 mag bluer. On the other hand, such an extreme assumption would have been unjustified. Nevertheless, this example gives an idea of the possible uncertainties involved.

5. COLOR-MAGNITUDE DIAGRAM

A color-magnitude diagram (CMD) has been generated (Fig. 2), where M_{130} is plotted versus the color index m_{130}-m_{346}. We labeled the eight R136a components in this figure, which have originally been resolved by Weigelt & Baier (1985). Interestingly, they are the brightest stars and also among the reddest. Their location in the CMD suggests that the brightest stars in R136 are concentrated in the center of the cluster. To further investigate the question, we have analyzed the star brightness distribution of the cluster as a function of the distance from the center. As a reference magnitude, we have taken the average M_{130} of our observed CMD ($M_{130M} \simeq -8$). We find that out of the 79 stars within 3″ from the center which are brighter than -8, 35 fall within a 1″ radius circle, 32 in the annulus between 1″ and 2″ from the center, and 12 in the outer region (up to 3″). From these numbers we derive a density of 11.1, 3.4, and 0.8 "*bright*" stars per square arcseconds, respectively. This is clear evidence for the scarcity of bright stars in the more external regions and is not due to a completeness effect, which would rather affect the low-luminosity objects. Another characteristic of this CMD is the noticeable dispersion in color of the components, at all luminosity levels. While for faint objects photometric errors can possibly dominate this dispersion, the color spread of bright stars is more likely to be generated by extinction effects across the cluster. We notice, however, that in the UV CMDs are always characterized by larger color dispersions than in the visible (see, e.g., De Marchi, Paresce, & Ferraro 1993 for the case of globular clusters).

The completeness of faint stars in our CMD is severely limited by the crowding of the inner region of the cluster and increases rapidly with the distance from the center. Rather than attempting to define a completeness correction factor per magnitude interval, which would be somewhat arbitrary, we prefer to give the detected limiting magnitude as a function of the distance from the center. This function is plotted in Figure 3. It converges to the limiting magnitude defined by the image depth for distances larger than $\simeq 2\farcs5$. Adopting the conservative criterion of discarding all stars with a S/N ratio less than 2.5 in the peak, this limiting magnitude is estimated to be $M_{130_{lim}} \simeq -5.3$.

The dashed line running across our CMD (Fig. 2) represents the magnitude limits below which the peaks of the stellar images (in either filter) rise less than 4 σ over the frame-averaged sky level. It is almost totally dominated by the F346M frame, which is characterized by a lower average S/N with respect to the F136M. This limit clearly defines the region below which our photometry begins losing objects and is a very strong function of the color.

6. THEORETICAL ISOCHRONES

The CMD can be compared to a set of theoretical isochrones, which have been computed using evolutionary

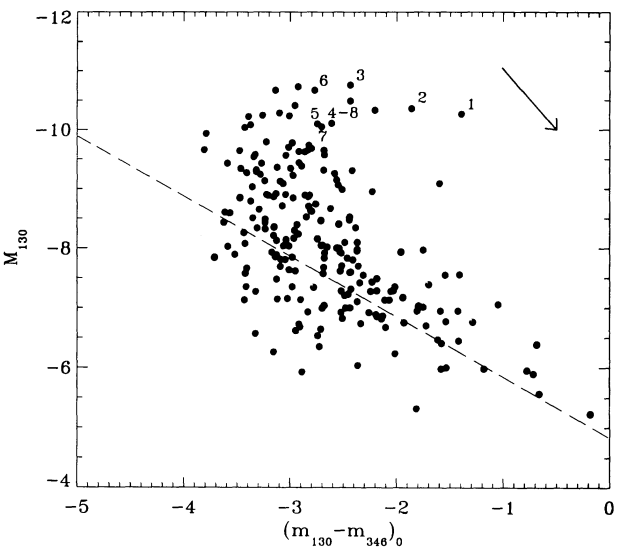

FIG. 2.—Color-magnitude diagram of the R136 cluster. M_{130} is plotted vs. the dereddened color index $(m_{130}$-$m_{346})_0$. The eight R136a components originally resolved by Weigelt & Baier (1985) have been individually marked. We also display the direction of the reddening vector, whose length, for reference, corresponds to $E(B-V) = 0.1$. The dotted line drawn across the diagram indicates the 4 σ detection limit.

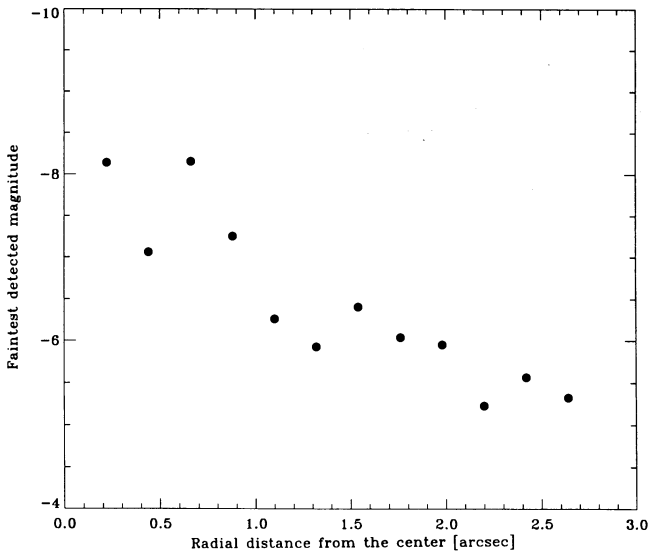

FIG. 3.—Graphic representation of the completeness of our photometry: the plot displays the limiting magnitude for any given distance from the cluster center. The curve converges toward the true limiting magnitude ($M_{130} = -5.3$) of the frame at distances larger than 2".5 for the center.

models by Maeder (1990). These models cover the metallicity range $0.1\ Z_\odot \leq Z \leq 2\ Z_\odot$ for stars with initial mass between 15 and 120 $M_\odot$. Models with solar metallicity published by Maeder & Meynet (1988) are used to extend the isochrones to stellar masses below 15 $M_\odot$. Since metallicity-dependent mass-loss effects are negligible at such low masses, Maeder's & Meynet's models can also be adopted for stars with $M < 15\ M_\odot$ having $Z \neq Z_\odot$. LTE model atmospheres with line blanketing from Kurucz (1992) are adopted for stars which are not in their W-R phase. W-R stars are defined in the same way as in Maeder (1990): effective temperatures $T_{\rm eff}$ are higher than 25,000 K, and the surface hydrogen content is less than 0.4 by mass. The emergent fluxes of W-R stars are calculated with the theoretical continuum energy distributions of Schmutz, Leitherer, & Gruenwald (1992) and Schmutz et al. (1993). The non-LTE radiative transfer in the expanding atmosphere is solved in spherical geometry. Only helium is considered. A complete model is characterized by the effective temperature $T_{\rm eff}$, radius R (both calculated where the outflow velocity is still subsonic), mass-loss rate $\dot{M}$, and the velocity field. These models overcome many of the deficiencies associated with static LTE atmospheres when applied to W-R stars. An important difference of these models with respect to Kurucz's models is their significantly flatter Balmer continuum.

We compute the positions of the stars in the Hertzsprung-Russell diagram from the zero-age main-sequence (ZAMS) to their endpoint when they exhaust all their nuclear fuel. Coeval star formation is assumed, with no subsequent star formation. For each time- and mass-step we compute the stellar energy distribution of the stars. No effort is made to account for metallicity variations of the model atmospheres, for which we assume solar abundances. The consequences of different metal abundances for the continuum fluxes of hot stars, in the Balmer and Paschen continua are negligibly small (see Howarth & Lynas-Gray 1989). Metallicity does enter indirectly in the isochrones, however, via the modified evolutionary tracks at different chemical composition. Effective temperatures and radii of non–W-R stars are taken directly from the evolutionary models. Temperatures and radii for W-R stars are corrected for wind-blanketing effects as described by Schmutz et al. (1992). A general outline of the method has been given by Leitherer, Gruenwald, & Schmutz (1993).

The model atmospheres have then been renormalized to derive the expected fluxes in the FOC bandpasses, which have been converted into the corresponding UV *HST* instrumental magnitudes. This is done by running the theoretical spectra through the FOC-specific FOCSIM simulation software for each chosen filter.

In Figure 4 we show an example of the resulting isochrones in the ultraviolet color-magnitude diagram. In order to high-

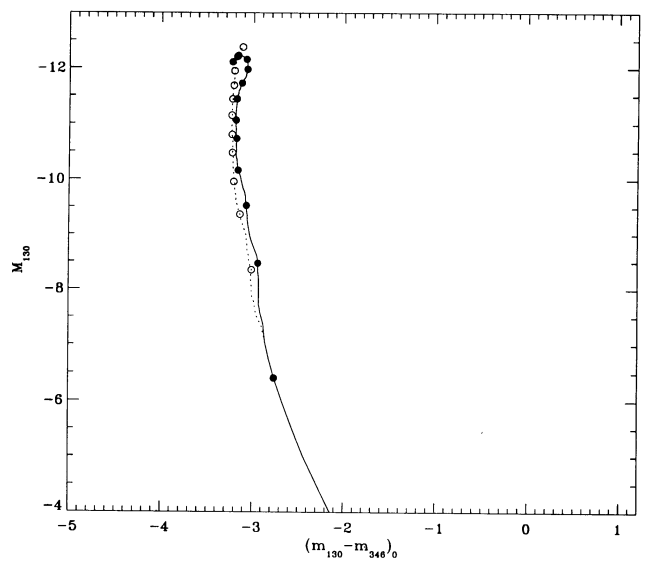

FIG. 4*a*

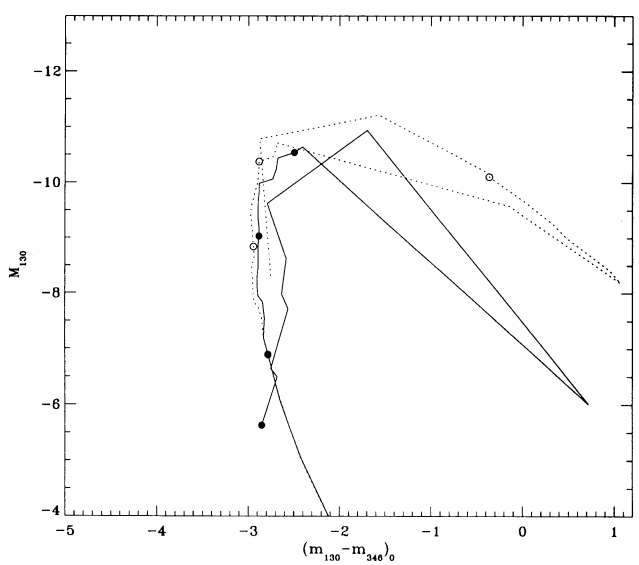

FIG. 4*b*

FIG. 4.—Four isochrones are shown here: one pair at an age of 2 Myr (*a*), with $Z = Z_\odot$ and $Z = 0.25\ Z_\odot$, respectively; the other pair at an age of 5 Myr (*b*) and the same two metallicities. Masses are marked by circles (open circles for $Z = 0.25\ Z_\odot$ and filled circles for $Z = Z_\odot$), starting from $10\ M_\odot$, with a sampling of $10\ M_\odot$. The differences between isochrones of the same age is entirely due to the evolutionary models and not to the model atmospheres.

light the fundamental properties of the models, we included four isochrones in this figure: one pair having an age of 2 Myr with $Z = Z_\odot$ and $Z = 0.25\ Z_\odot$, respectively; the other pair having an age of 5 Myr and the same two metallicities. The differences between isochrones of the age but different Z is entirely due to the evolutionary models, and not due to the model atmospheres. Stars on or close to the main sequence have rather similar M_{130} magnitudes and m_{130}-m_{346} colors. During later evolutionary phases, Z-dependent mass loss in the models determines the amount of hydrogen-rich layers removed from the stellar surface. Therefore the colors and magnitudes of the most massive stars are rather sensitive to those particular evolutionary phases and to the metallicity. During most of the main-sequence lifetimes, however, isochrones with $Z_\odot$ and $0.25\ Z_\odot$ are nearly indistinguishable if uncertainties such as, for example, photometric errors or selective interstellar extinction are taken into account.

In this study we will use isochrones based on models with $Z = 0.25\ Z_\odot$. The chemical composition of young stars in the LMC is relatively uncertain (see Feast 1991). Spite & Spite (1991) discussed carbon, silicon, and oxygen abundances of young Galactic and LMC stars. LMC stars are less abundant than their Galactic counterparts by about 0.3 dex. However, this value refers to somewhat older objects than found in R136, which may have chemical composition closer to those H II regions surrounding them. H II regions in the LMC are less metal-rich by about a factor of 3 than Galactic H II regions. This suggests that the population of massive stars in R136 has a chemical composition which is most likely between 0.33 and $0.5\ Z_\odot$. The evolutionary models which are available to us are somewhat higher ($Z_\odot$) or somewhat lower ($Z_\odot$), and no convincing case could be made for or against either one. We selected the models with $Z = 0.25\ Z_\odot$ but note that the main conclusion of this study (the masses of the most massive stars) does not depend on this particular choice.

Figure 4 illustrates the degeneracy of the high-mass part of the CMD. The steep mass-luminosity relation ($L \propto M^{2.3}$ between 20 and 60 $M_\odot$; Maeder 1990) and weak sensitivity of ultraviolet colors for temperatures of massive stars make it difficult to discriminate between individual stellar masses if $M > 50\ M_\odot$. This problem becomes even more severe if visual CMDs, such as M_V versus $(U-B)$, are considered. Massey (1985) demonstrated that it is virtually impossible to discriminate between the most massive stars on the basis of photometry longward of the Balmer discontinuity. By using ultraviolet colors such as the ones discussed here, the color degeneracy of very massive stars can be removed to some degree and the stellar mass function can be studied on the basis of photometry without the need for additional spectroscopic data. This point becomes evident by comparing Figure 4 with the corresponding V versus $(U-B)$ CMD published for M31 by Massey, Armandroff, & Conti (1986). The intrinsic $(U-B)$ of stars in the mass range 20–60 $M_\odot$ is essentially constant. Conversely, $(m_{130} - m_{346})_0$ displays a significant variation with stellar mass.

7. THE AGE OF THE R136 CLUSTER

We compare the observed CMD to the theoretically derived set of isochrones in order to estimate the age and the mass spectrum of the cluster. The age of the R136 complex has been under debate. Savage et al. (1983) and Schmidt-Kaler & Feitzinger (1981) quote an age on the order of 2×10^6 yr for the "superluminous" object in the center of R135. This age estimate increased with the discovery of W-R features in the integrated spectrum of the cluster (Melnick 1985). Subsequently Meylan (1991) derived an age lower than 3×10^6 yr from ground-based CCD BV photometry. More recently, Campbell et al. (1992) argued that the presence of W-R stars in the core of R136 suggests an age of at least 3.5×10^6 yr, even though the core radius and brightness distribution would imply a much smaller relaxation time.

Walborn (1984) discussed the observational evidence for the existence of an age spread among the stars in the entire 30 Doradus region. However, the core of 30 Doradus is characterized by a coeval stellar population. Coeval star formation within R136 is supported on theoretical grounds. The linear size covered by our FOC images is approximately $d \simeq 5$ pc. A typical time scale associated with the star-formation process is given by $t = d/v$, where v is taken as the sound speed. This suggests age spreads of less than 0.5 Myr, which is short as compared to the evolutionary time scale of the stars formed.

As already outlined above, the presence of W-R stars gives a lower limit of at least 2 Myr for the age of R136. An upper limit for the age can be inferred from the nature of the W-R stars in R136. They are of type WNL, a hydrogen-rich W-R subclass, which is usually associated with very massive progenitors > 50 $M_\odot$ (Humphreys, Nichols, & Massey 1985). The evolutionary time scale of such stars is shorter than 5 Myr. Further evidence against an age significantly above 5 Myr comes from the lack of red supergiants in R136. Stars with ZAMS masses around 40 $M_\odot$ evolve into red supergiants after about 5 Myr (see Maeder 1990). The presence of red supergiants has been used to characterize nearby star-forming regions like $h + \chi$ Per (Walborn 1991), as well as more distant starbursts (Terlevich et al. 1990). No red supergiants are detected on our FOC images, although they should be above our detection limit in the F346M frame. This argument, however, is not as robust as the previous one. If very massive stars (e.g., above $M = 20\ M_\odot$) had never formed in R136, the occurrence of the first red supergiants may be as late as 10 Myr after the onset of the star-formation episode. On the other hand, the presence of WNL stars essentially rules out such a low cutoff mass. Therefore, the presence of WNL stars and the lack of red supergiants taken together place a relatively firm upper limit of 5 Myr on the age of R136. The most likely age of R136 is between 2 and 4 Myr.

In Figure 5 we overlay isochrones corresponding to 3 and 4 Myr and $Z = 0.25\ Z_\odot$ on our observed CMD. A sampling of 10 $M_\odot$ has been adopted for display purposes. For the two time intervals considered, the fit between the observed and theoretical distributions is in better agreement for main-sequence stars fainter than $M_{130} \simeq -10$ than for the brightest region of the diagram. In other words, we do not observe the theoretically expected population of very bright and very massive stars which have recently left the main sequence and are evolving toward the supergiant and W-R phases. This could be due to several reasons:

R136 is significantly older than 4 Myr, and the most massive stars have already exploded as supernovae.

We are not accounting properly for a differential absorption effect across the image. Interstellar absorption may be more enhanced toward the center where the brightest objects are concentrated.

The most massive stars in R136 have ZAMS masses less than about 50 $M_\odot$. We do not observe particularly massive stars just because they have never formed, differently from what is observed in other regions in 30 Doradus.

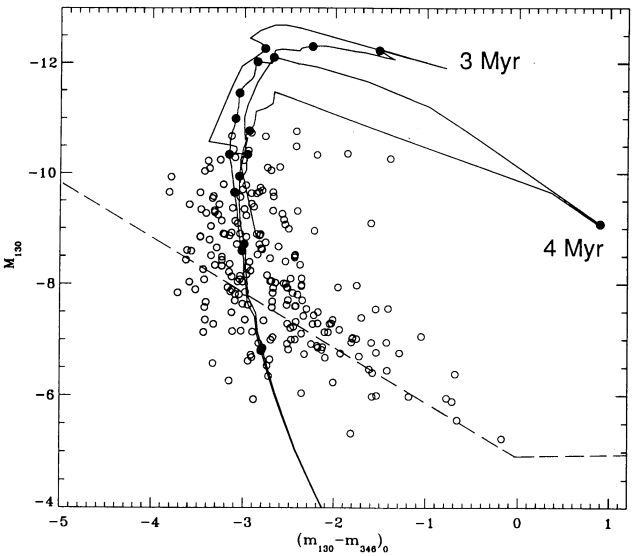

FIG. 5.—Isochrones corresponding to 3 and 4 Myr and $Z = 0.25\ Z_\odot$ are superposed on the observed CMD. Filled circles along the isochrones represent mass steps starting from 10 $M_\odot$ (at $M_{130} \simeq -6.8$), with a sampling of 10 $M_\odot$ adopted for display purposes. For the two time intervals considered, the fit between the observed and theoretical distributions is in better agreement for main-sequence stars fainter than $M_{130} \simeq -10$, than for the brightest region of the diagram. The dashed line indicates the 4 σ detection limit.

From our previous discussion we can rule out the possibility of a much older age of R136. Additional constraints on the age of R136 are imposed by the X-ray emission observed by the *Einstein* satellite (Wang & Helfand 1991). HRI data at 3″ resolution suggest a total X-ray luminosity of about 2×10^{37} ergs s^{-1} for R136. The most likely interpretation is an origin in the interstellar medium due to the interaction of powerful stellar winds and/or supernovae with the ambient interstellar gas. If R136 has an age of only a few Myr, only few—if any—supernova events should have resulted from the current star-formation episode. On the other hand, large numbers of hot stars in the mass range around 40 $M_\odot$ are present in R136, and their winds can provide the energy input to account for the observed X-ray emission.

After ruling out a much higher age of R136, we will discuss the effects of differential absorption and of an upper cutoff mass in the IMF.

8. A POSSIBLE DIFFERENTIAL ABSORPTION

In order to investigate the presence of differential absorption across the cluster, we compared the projected surface brightness as a function of the distance from the center in both bandpasses. We first derived the position of the cluster center on the best S/N image taken in the F130M, using a mirror-autocorrelation technique, a very robust method which takes full advantage of the two-dimensional information present in the image, as described by Djorgovski (1986). We then assumed the center to be the same for both filters. The error on the obtained location, marked in Figure 1, can be estimated to be approximately 0″.07, with negligible consequences on the subsequent calculations.

The determination of the radial brightness profile was performed by dividing the image into 21 equally spaced concentric annuli of increasing radius up to 2″.6. This limit is imposed by the size of our field of view. The counts falling in the annuli were summed to provide an integrated surface brightness as a function of the distance from the measured center. The dispersion σ of these sums was obtained by subdividing each annulus into 8 sectors and calculating the dispersion of the eight values within the same annulus. We emphasize we used directly photon counts rather than star counts, to avoid incurring into crowding effects (King 1968) which could be hard to estimate and correct for.

The relationship between the angular scale and the linear scale in the cluster is obtained by using the determination of distance for the 30 Doradus region as given by Panagia et al. (1991), $m_v - M_v = 18.54 \pm 0.13$, or $d = 51.2 \pm 3.1$ kpc. With this relationship, 1 pc corresponds to 4″ in our image.

We have fitted the light distribution in R136 using the simple relationship derived by King (1962):

$$I = \frac{I_0}{1 + (r^2/r_c^2)} . \tag{5}$$

This relation is usually adopted in the literature for globular clusters but it still holds as a first approximation for open clusters (King 1980). The model is characterized by the unique geometrical parameter r_c, called *core radius*, that is the projected distance from the center of the cluster to the location where the density drops to one half of the central value. I_0 is a normalization factor. From the raw images, we obtain for the core radius $r_c = 1''.0 \pm 0''.1$ in the F130M filter and $r_c = 0''.8 \pm 0''.1$ in the F346M. Both these values are affected by the presence of the spherical aberration that degrades the resolution and, by redistributing the light of an unresolved source over a 2″ radius halo, broadens the overall profile.

Rather than using deconvolved images for our determination, however, we prefer to measure the radial profile on the raw frames and then deconvolve it to remove the effect of the aberrated PSF. With this technique, the *true* core radius for the F130M results to be $r_c = 0.15 \pm 0.03$ pc ($0''.6 \pm 0''.1$), while for the F346M we have $r_c = 0.10 \pm 0.03$ pc ($0''.4 \pm 0''.1$). Previous determinations were 0.05 pc (0″.2) given by Chu (1984) and Chu, Cassinelli, & Wolfire (1984), 0.32 pc (1″.25) given by Moffat & Seggewiss (1983), and 0.21 pc (0″.82) given by Moffat et al. (1985).

Recently, Elson et al. (1992) derived $r_c = 0.1$ pc (0″.5) by averaging the results of the deconvolution of two low S/N FOC images taken through the F346M and F410M filters, respectively. We note that the F346M image analyzed by Elston et al. is not the one we present in this paper, but is a less deep exposure taken at (approximately) the same time. Campbell et al. (1992) show, by using a F336W *HST*-PC image, that the surface brightness profile of R136 is consistent with a pure power law of index $\gamma = -1.72 \pm 0.06$, but at the same time they do not rule out the possibility of a small core ($r_c = 0.06$ pc, i.e., 0″.25). It must be noted, however, that these authors generate the radial profile by binning their stellar photometry: it is clear that their profile suffers from the effect of completeness decreasing toward the center and as consequence is not representative of the actual light distribution in the cluster.

Our observed (not deconvolved) surface brightness profiles, suitably normalized, are plotted in Figure 6, where the difference between the two is also shown. It is immediately noticed that up to 0″.3 the F346M profile is systematically steeper than the one for the F130M filter, while for distances larger than 0″.4 the agreement between the two profiles is well within the

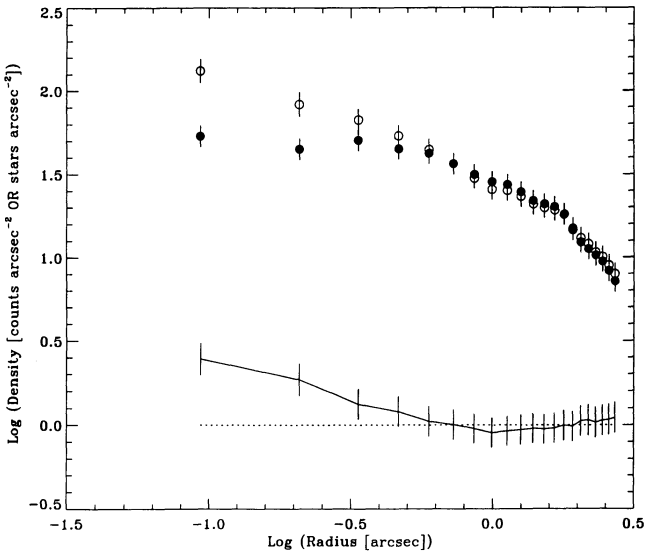

FIG. 6.—The observed (not deconvolved) surface brightness distributions in the F130M (*filled circles*) and F346M (*open circles*), suitably normalized. The difference between the two is also shown. The F346M profile is systematically steeper than the one for the F130M filter up to 0".3, while for distances larger than 0".4 the agreement between the two profiles is well within the errors.

errors. This seems to indicate that the stars in the central 0".3 of R136 are redder than we would expect. This effect has also been observed by Campbell et al. (1992) who attributed their findings to an offset in the flat-field normalization of their CCD frames.

On the other hand, this effect could be understood in the case of a variable absorption across the cluster surface, due, for instance, to the presence of dust clouds, denser at the center than outside. In the assumption that the nebular dust in these clouds follows the absorption law presented in § 4, we can derive from Figure 6 the amount of *additional* $E(B-V)$ required to account for the differential absorption, as a function of the radial distance, for the stars in the innermost 0".3 of the cluster core. We find that for R136a_1 and R136a_2 (following the nomenclature introduced by Weigelt & Baier 1985) the total $E(B-V)$ should be ~ 0.73 and ~ 0.65, respectively. Given the average observed $B-V \simeq 0.14$ (Moffat et al. 1985), this would imply the unlikely $(B-V)_0$ values of ~ -0.59 and ~ -0.51, respectively, which are by far too blue to agree with the observed or predicted values for any stellar object.

The amount of *additional* $E(B-V)$ would be less if the distribution of the matter causing this differential absorption followed a steeper law than the one we used. However, we have no means to test this hypothesis at this moment. For the purpose of interpreting our results, we will therefore discard this possibility and assume that the $m_{130} - m_{346}$ colors of the stars within 0".3 of the cluster center are true and caused by evolutionary effects alone. In this case the redder colors of the most luminous stars can be understood in terms of bolometric luminosity correction: the most luminous stars are more evolved and have a redder color.

9. THE UPPER MASS CUTOFF IN R136

We do not attempt to derive the initial mass function (IMF) for the region covered by our images. In principle, ultraviolet photometry partially overcomes the color degeneracy of hot stars and is suitable to assign effective temperatures, and hence stellar masses. However, the central region of 30 Doradus contains a large fraction of evolved, peculiar objects (see Walborn 1986 for a list of spectral types), which makes an extrapolation back to the ZAMS highly uncertain. Therefore we will only address the apparent deficiency of stars with masses above $\sim 50\ M_\odot$ in our observed CMD.

Incompleteness at faint magnitudes sets in at $M_{130} \simeq -7$, corresponding to a ZAMS mass of $\sim 10\ M_\odot$ (see Fig. 5). All stars visible in the CMD are expected to be members of the LMC and not Galactic foreground stars. This follows from predictions of the stellar number densities at the Galactic latitude of the LMC (Bahcall & Soneira 1980). Figure 5 contains 221 stars. We can estimate the expected number of stars above some mass limit if an assumption for the IMF is made. Studies of the IMF in sites of massive star formation resulted in slopes between -2 and -2.6 (Massey & Thompson 1991; Parker 1992). Here we adopt a classical Salpeter (1955) IMF with a slope of -2.35. This IMF predicts 11.2 for the ratio of the number of stars in the mass interval $10\ M_\odot < M < 50\ M_\odot$ over those within $50\ M_\odot < M < 120\ M_\odot$. Applied to Figure 5, one would expect about 20 stars with ZAMS masses above $50\ M_\odot$, that is, $M_{130} < -11$, given the observed number of stars between 10 and $50\ M_\odot$. These stars are not observed. Although we are dealing with small-number statistics (as is usually the case at the high-mass end of the IMF), the lack of extremely massive stars in R136 cannot be disputed. This result is consistent with earlier results by Campbell et al. (1992) who note that none of the stars in R136 is remarkable in terms of its luminosity. Similarly, Moffat et al. (1985) made use of ground-based photometry to conclude that R136 does not contain extraordinarily bright stars. Our observations further substantiate these results. Parker (1992) did a photometric and spectroscopic census of the 30 Doradus region. He finds evidence for a significant steepening of the IMF toward the high-mass end. This may also suggest a real deficiency of very massive stars in this region.

The brightest stars in our CMD are the individual components of R136a. They are labeled a_1 through a_8, following the nomenclature introduced by Weigelt & Baier (1985). Ground-based (Moffat et al. 1987) and *HST* (Campbell et al. 1992) observations suggest that some, if not most, stars are in a fairly advanced evolutionary stage, as evidenced by strong wind emission lines. This is consistent with their location in the CMD with respect to the theoretical isochrones. The colors of R136a_1 through a_8 can be understood if the stars are either very evolved blue supergiants or W-R stars. It is difficult to estimate the initial mass of the objects purely from their position in the CMD. Although formally a ZAMS mass of 30–40 $M_\odot$ could be assigned, we emphasize that essentially *all* W-R stars pass through this part of the CMD, irrespective of the progenitor mass. This is a consequence of the mass loss versus mass relation used in the evolutionary tracks, which channels most W-R stars through the same part of the Hertzsprung-Russell diagram.

If a_1 through a_8 are considered in the context of the entire R136 population, their masses can be constrained to some degree. We recall that there are no stars on or close to the ZAMS above about $50\ M_\odot$. If a_1 through a_8 had progenitor masses above $\sim 80\ M_\odot$, we would expect a significant main-sequence population in the mass range $50\ M_\odot < M < 80\ M_\odot$ as the stellar lifetimes decrease with mass. This is not observed. Therefore it is unlikely that the individual components of

R136a had masses on the ZAMS larger than approximately 80 $M_\odot$. Most probably they originated from stars of masses around 50 $M_\odot$.

This estimate for the ZAMS masses of a_1 through a_8 is considerably lower than thought previously, even after the multiplicity of R136a was recognized. For instance, Walborn (1986) suggested an initial mass of about 250 $M_\odot$ for a_1 based on the argument that a_1 is about 1 mag brighter in M_V than HD 93129A, a luminous galactic star of type O3If, for which a mass of $117 \pm {}^{57}_{38}\ M_\odot$ gas been suggested (Kudritzki et al. 1991).

The ZAMS-mass estimate of the brightest components of R136a must be revised downward with the new *HST* photometry. For instance, we find an absolute magnitude of -8.87 in the F346M passband for a_1. It is difficult to transform this magnitude into the standard Johnson system. Therefore we make use of Campbell et al.'s *HST* photometry in the F555W passband for a comparison with previous ground-based V photometry. The F555W filter of the PC is sufficiently close to the Johnson V for a meaningful comparison. Campbell et al. observe the following magnitudes in the F555W passband: a_1: 12.78; a_2: 13.09; a_3: 12.87; a_4: 13.56; a_5: 13.73; a_6: 1406; a_7: 13.78; a_8: 14.28. Let us note here again that a_4 and a_8 are here treated as two separate stars while we find they indeed are one, unresolved object. The total magnitude of all eight components is 11.14. Moffat et al. (1985) derived a lower (bright) limit of $V > 10.95$, which is consistent with the *HST* data. In contrast, earlier ground-based photometry by Schmidt-Kaler & Feitzinger (1981) gave $V = 10.77$ for R136a. This value is probably affected by crowding and background problems. The superior *HST* photometry results in a V-magnitude which is fainter by 0.37 mag for the integrated magnitude of all eight components. Our ultraviolet photometry as well as Campbell et al.'s visual photometry result in rather similar magnitudes of all eight components compared to earlier studies. The spread in magnitude is less than 1.5. The same result with respect to the magnitude spread has been found by Pehlemann, Hauffmann, & Weigelt (1992). In contrast, Weigelt & Baier (1985) estimated rather similar brightness for a_1, a_2, and a_3, but up to 3 mag fainter values for the other components. Their estimates let the three brightest components appear brighter (and therefore more massive) with respect to the fainter components than supported by *HST* photometry. These factors taken together account for the downward revision of the ZAMS mass of $R136a_1$.

We obtain $M_{F555W} = -7.16$ for a_1, using $A_V = 1.39$ and $V_0 - M_{F555W} = 18.55$. This is essentially the same absolute magnitude as of HD 93129A ($M_V = -7.0$; Humphreys 1978). Note that our derived M_V for a_1 would be even lower if we adopted Walborn's (1986) absorption correction of $A_V = 1.2$. We emphasize that the error bars for M_V of HD 93129A are large: (1) the V photometry of HD 93129A ($V \simeq 7.3$) has an uncertainty of 0.1 mag due to the close companion HD 93129B; (2) the extinction correction is very high, being $A_V \simeq 1.7$; (3) the distance module of Trumpler 14 may be 0.4 mag smaller than adopted here. (See Walborn 1973, 1982 for a thorough discussion.) Therefore no significant M_V difference between $R136a_1$ and HD 93129A can be claimed. *Within the uncertainties, $R136a_1$ and HD 93129A have the same absolute visual magnitudes.*

Although differences between the photometric systems preclude any significant comparison between absolute magnitudes in the F346M and U passbands, we mention that these data also suggest similar magnitudes for $R136a_1$ and HD 93129A. With $U = 6.81$, $A_U = 2.79$, and a distance module of 12.7 we find $M_U = -8.7$ for HD 93129A, in close agreement with $M_{346} = -8.9$ for $R136a_1$. The same cautionary remarks about the uncertainties as in the previous paragraph apply here. We also note that if there were a significant brightness difference between the two stars (e.g., by 0.5 mag), this would immediately translate into a large difference in mass (up to a factor of 1.5).

Spectral morphology suggests that the atmosphere of $R136a_1$ is dominated by stellar-wind effects to a much larger extent than HD 93129A (Walborn et al. 1992). Massive stars with very dense winds, such as W-R stars, have a redder Balmer continuum than stars with the same M_V but less dense winds (Schmutz 1991). Therefore the bolometric correction of $R136a_1$ will be smaller than the one for HD 93129A so that $R136a_1$ will have a smaller bolometric luminosity than HD 93129A. Consequently it is expected that the ZAMS mass of $R136a_1$ is lower than $117 \pm {}^{57}_{38}\ M_\odot$, the value suggested for HD 93129A. This is consistent with our mass estimate of 50 $M_\odot$ derived from isochrone fitting.

The mass of HD 93129A was derived from a spectroscopic fine analysis. Herrero et al. (1992) found evidence that evolutionary masses of very evolved stars are systematically higher than the corresponding spectroscopic masses. The reason for this discrepancy is yet unknown. If evolutionary masses were systematically too high, then the masses of the most massive stars in R136 would be even lower.

10. CONCLUSIONS

A new set of ultraviolet ($\lambda \simeq 1300$ Å, $\lambda \simeq 3400$ Å), *HST* FOC images of R136 has been used to derive its UV CMD. Ultraviolet colors of hot stars are less affected by the color degeneracy of the Rayleigh-Jeans tail encountered in visual colors. It is virtually impossible to discriminate between the most massive stars on the basis of visual photometry longward of the Balmer discontinuity.

The CMD has been compared to a set of theoretical isochrones, which have been computed using evolutionary models by Maeder (1990), to cover masses up to 120 $M_\odot$. There is very good agreement for main sequence stars fainter than $M_{130} \simeq -10$. In contrast, we do not observe any brighter stars.

From the presence of WNL stars, we derive a lower limit to the age of R136 of 2 Myr. The absence of evolved, red supergiants imposes an upper limit of approximately 4 Myr on the age. The main-sequence turnoff for isochrones in the age range 2–4 Myr is only consistent with the observations if the mass of the most massive stars observed is around 50 $M_\odot$.

We studied the effects of possible differential absorption present in the core of the cluster, which might produce an underestimate of the luminosity and, therefore, of the mass. This interpretation has been discarded, though, as the color difference observed in the light distribution of the cluster in the two filters would suggest an $E(B-V)$ which by far exceeds the observed and predicted values for stars in the same spectral class of the R136 core members.

We conclude that the lack of extremely luminous stars in R136, already suspected from ground-based observations (Moffat et al. 1985) and more recently from *HST* observations (Malumuth & Heap 1992; Campbell et al. 1992), is due to an intrinsic deficit of stars with ZAMS masses above $\simeq 50\ M_\odot$ if a standard Salpeter IMF is extrapolated upward from the mass interval $10\ M_\odot < M < 50\ M_\odot$. The individual components of

R136a are the most luminous—and presumably among the most massive—stars in the R136 region. Their ZAMS masses may be as high as 80 $M_\odot$ but values around 50 $M_\odot$ are more likely.

The availability of very high spatial resolution data, both from the ground (NTT, Heydari Malayeri & Melnick 1992), and from space (*HST*) have in many cases significantly affected our perspective of various astrophysical objects: examples are the discovery of the ring around SN 1987A (Wampler et al. 1990; Panagia et al. 1991), the high number density of blue stragglers in the resolved cores of globular clusters (Paresce et al. 1991) or the first evidence of a dust disk in the nucleus of NGC 4261 (Jaffe et al. 1993). Similarly, in the case of 30 Doradus, severe crowding, combined with seeing effects, had led in the past to a significant overestimate of the stellar masses of individual objects.

We found that the most massive stars in R136 have ZAMS masses of around 50 $M_\odot$. The very early suggestion of the existence of a supermassive star with mass above 1000 $M_\odot$ (Cassinelli et al. 1981) in the core of R136 is revised by an order of magnitude in the present study. We emphasize that our conclusions refer only to R136, the central region of 30 Doradus. Our result does not exclude that higher mass stars exist in the larger 30 Doradus region. What is the impact of this result on our current general understanding of the mechanism of formation of very massive stars, and its dependence on the physical characteristics of the local environment? If this upper mass cutoff is also representative for other sites of massive star formation, this implies that stars significantly more massive than $M = 100\ M_\odot$ *just do not exist*. The reason for this is currently not fully understood.

It has been suggested that stars above this mass limit would rapidly disintegrate after formation by radiation pressure or nonradial pulsations (Appenzeller 1987). Alternatively, high-mass star formation may already be prohibited during the fragmentation process of molecular clouds (Silk 1986).

In the vicinity of the Sun ($d < 3$ kpc), the most massive stars have main-sequence masses around 60–100 $M_\odot$ (Leitherer 1991), from both observational data and theoretical considerations. Studies of the emission-line spectrum of H II regions in a large number of galaxies (e.g., Campbell 1988; Viallefond 1986) show different results, and have led to a correlation between metal abundance and the temperature of the ionizing stars. Metal-poor H II regions are associated with hotter stars than metal-rich H II regions. Utilizing a $T_{\rm eff}$ versus luminosity and mass relation, this can be translated into a relation between metal content and the typical mass of stars contributing to the ionization. This result would suggest that metal-rich H II regions ($Z > Z_\odot$) have a deficit of very massive ($M > 25\ M_\odot$) stars compared to metal-poor H II regions (Lenzuni & Panagia 1993, but see also McGough 1991). Additional evidence for this hypothesis comes from infrared studies of metal-rich starburst regions (Rieke 1991; Joseph 1991; Doyon, Puxley, & Joseph 1992), which indicate $M_{\rm up} \simeq 25\ M_\odot$ in a sample of starburst nuclei. These results imply that the upper mass spectrum in some regions of violent star-formation activity is dramatically different from its properties in the solar vicinity. Our result does not strongly support this correlation, as we are finding less extremely massive stars in R136 (where the metal content is at least a factor 2 lower than solar) than in the solar neighborhood. Nevertheless, R136 is an outstanding star-formation laboratory. We found a total of $\sim$165 stars more massive than 10 $M_\odot$ within the central 3″ radius. This yields a space density of ~ 125 stars per pc^3.

At present no high spatial resolution study is available to investigate the lower end of the mass function in the cluster. Observational evidence hints at a lower mass cutoff of the initial mass function in starburst regions of about 3 $M_\odot$ (Riekel 1991). In the case of R136 we would expect the existence of a similar cutoff. The time scale of pre–main-sequence stars to reach the ZAMS is roughly given by Helmholtz-Kelvin time scale $\tau \propto M^2 L^{-1} R^{-1}$. Assuming coeval star formation, an age of 3 Myr implies that stars less massive than 2–3 $M_\odot$ have not yet reached the ZAMS. The corresponding M_V of stars in this mass range is approximately 0 mag, which would result in an apparent magnitude of $V \approx 20$. Deep, high-spatial resolution imaging of R136 in visible bands is required to detect the presence of such a cutoff. This project is feasible with *HST*.

We are very grateful to Nino Panagia and Nolan Walborn for several useful comments on the original manuscript. We would also like to thank Dietrich Baade, the referee, for a thorough analysis of the paper.

REFERENCES

Appenzeller, I. 1987, in Instabilities in Luminous Early-Type Stars, ed. H. J. G. L. M. Lamers & C. W. H. de Loore (Dordrecht: Reidel), 55
Ardeberg, A. 1976, A&A, 127, 113
Bahcall, J. N., & Soneira, R. M. 1980, ApJS, 44, 73
Barbieri, C., De Marchi, G., & Ragazzoni, R. 1991, in The First Year of HST Observations, ed. A. L. Kinney & J. C. Blades (Baltimore: STScI), 253
Braunsfurth, E., & Feitzinger, J. V. 1983, A&A, 127, 113
Brunet, J. P. 1975, A&A, 43, 345
Burrows, C. J., Holtzman, J. A., Faber, S. M., Bely, P. Y., Hasan, H., Lynds, C. R., & Schroeder, D. 1991, ApJ, 369, L21
Campbell, A. 1988, ApJ, 335, 644
Campbell, B., et al. 1992, AJ, 104, 1721
Cassinelli, J. P., Mathis, J. S., & Savage, B. D. 1981, Science, 212, 1497
Chu, Y.-H. 1984, IAU Symp. 108, Structure and Evolution of the Magellanic Clouds, ed. S. van der Bergh & K. S. de Boer (Dordrecht: Reidel), 259
Chu, Y.-H., Cassinelli, J. P., & Wolfire, M. J. 1984, ApJ, 283, 560
Chun, M. S. 1978, AJ, 83, 1062
De Marchi, G., Paresce, F., & Ferraro, F. R. 1993, ApJS, 85, 293
Djorgovski, S. 1986, IAU Symp. 126, The Harlow-Shapley Symp. on Globular Cluster Systems in Galaxies, ed. J. E. Grindlay & A. G. Davis Phillip (Dordrecht: Reidel), 333
Doyon, R., Puxley, P. J., & Joseph, R. 1992, ApJ, 397, 117
Elson, R. A. W., Schade, D. J., Thomson, R. C., & Mackay, C. D. 1992, MNRAS, 258, 103
Feast, M. W. 1991, in IAU Symp. 148, The Magellanic Clouds, ed. R. Haynes & D. Milne (Dordrecht: Kluwer), 1
Feitzinger, J. V., Schlosser, W., Schmidt-Kaler, Th., & Winkler, C. 1980, A&A, 84, 50
Fitzpatrick, E. L. 1985, ApJ, 299, 219
Fitzpatrick, E. L., & Savage, B. D. 1984, ApJ, 279, 578
Gilmozzi, R. 1990, Instr. Sci. Rep. WFPC 90-007
Greenfield, P., et al. 1991, SPIE, 1494, 16
Herrero, A., Kudritzki, R. P., Vilchez, J. M., Kunze, D., Butler, K., & Haser, S. 1992, A&A, 261, 209
Heydari Malayeri, M., & Melnick, J. 1992, A&A, 258, L13
Howarth, I. D., & Lynas-Gray, A. E. 1989, MNRAS, 240, 513
Humphreys, R. M. 1978, ApJS, 38, 309
Humphreys, R. M., Nichols, M., & Massey, P. 1985, AJ, 101
Isserstedt, J. 1975, A&A, 41, 175
Jaffe, W., Ford, H. C., Ferrarese, L., van den Bosch, F., & O'Connell, R. W. 1993, Nature, 364, 213
Joseph, R. 1991, in Massive Stars in Starbursts, ed. C. Leitherer, N. R. Walborn, T. M. Heckman, & C. A. Norman (Cambridge: Cambridge Univ. Press), 259
King, I. R. 1962, AJ, 66, 384
———. 1968, AJ, 73, 456
———. 1980, IAU Symp. 85, Star Clusters, ed. J. E. Hesser (Dordrecht: Reidel), 139

Kudritzki, R., Gabler, R., Kunze, D., Pauldrach, W. A., & Puls, J. 1991, in Massive Stars in Starbursts, ed. C. Leitherer, N. R. Walborn, T. M. Heckman, & C. A. Norman (Cambridge: Cambridge Univ. Press), 59
Kurucz, R. L. 1992, IAU Symp. 149, The Stellar Populations of Galaxies, ed. B. Barbuy & A. Renzini (Dordrecht: Kluwer), 225
Leitherer, C. 1991, in Massive Stars in Starbursts, ed. C. Leitherer, N. R. Walborn, T. M. Heckman, & C. A. Norman (Cambridge: Cambridge Univ. Press), 1
Leitherer, C., Gruenwald, R., & Schmutz, W. 1993, in Physics of Nearby Galaxies, ed. T. X. Thuan, C. Balkowski, & J. T. T. Van (Paris: Editions Frontières), in press
Lenzuni, P., & Panagia, N. 1993, ApJ, submitted
Lortet, M.-C., & Testor, G. 1988, A&A, 194, 11
———. 1991, A&AS, 89, 185
Maaswinkel, F., Bortoletto, F., Buonanno, R., Buzzoni, B., D'Odorico, S., Gilli, B., Huster, G., & Nees, W. 1988, ESO Conference on Very Large Telescopes and Their Instrumentation, ed. M. H. Ulrich (Garching: ESO), 751
Mader, A., & Meynet, G. 1988, A&AS, 76, 411
Maeder, A. 1990, A&A, 84, 139
Malumuth, E. M., & Heap, S. R. 1992, in Science with the *Hubble Space Telescope*, ST-ECF/STSScI Workshop, ed. P. Benvenuti & E. Schreier, 297
Massey, P. 1985, PASP, 97, 5
Massey, P., Armandroff, T. E., Conti, P. S. 1986, AJ, 92, 1303
Massey, P., & Thompson, A. B. 1991, AJ, 101, 1377
McGough, S. S. 1991, ApJ, 380, 140
McGregor, P. J., & Hyland, A. R. 1981, ApJ, 250, 116
Meaburn, J., Hebden, J. C., Morgan, B. L., & Vine, H. 1982, MNRAS, 200, 1P
Melnick, J. 1985, A&A, 153, 235
———. 1987, IAU Symp. 121, ed. E. Ye. Khachikian, K. J. Fricke, & J. Melnick (Dordrecht: Reidel), 545
Meylan, G. 1991, private communication
Moffat, A. F. J., Niemela, V. S., Phillips, M. N., Chu, Y.-H., & Seggewiss, W. 1987, ApJ, 312, 612
Moffat, A. F. J., & Seggewiss, W. 1983, A&A, 125, 83
Moffat, A. F. J., Seggewiss, W., & Shara, M. M. 1985, ApJ, 295, 109
Neri, R., & Grewing, M. 1988, A&A, 196, 338
Panagia, N., Gilmozzi, R., Macchetto, F., Adorf, H.-M., & Kirshner, R. P. 1991, ApJ, 380, L23
Paresce, F. 1992, FOC Instrument Handbook (Baltimore: STScI)
Paresce, F., et al. 1991, Nature, 352, 297
Parker, J. 1992, Ph.D. thesis, Univ. Colorado
Pehlemann, E., Hauffmann, K.-H., & Weigelt, G. 1992, A&A, 256, 701
Rieke, G. H. 1991, in Massive Stars in Starbursts, ed. C. Leitherer, N. R. Walborn, T. M. Heckman, & C. A. Norman (Cambridge: Cambridge Univ. Press), 205
Salpeter, E. E. 1955, ApJ, 182, L21
Savage, B. D., Fitzpatrick, E. L., Cassinelli, J. P., & Ebbetts, D. C. 1983, ApJ, 273, 597
Schmidt-Kaler, T., & Feitzinger, J. V. 1981, in ESO Workshop on The Most Massive Stars, ed. S. D'Odorico, D. Baade, & K. Kjär (Garching: ESO), 105
Schmutz, W. 1991, in IAU Symp. 143, Wolf-Rayet Stars and Interrelations with Other Massive Stars in Galaxies, ed. K. van der Hucht & B. Hidayat (Dordrecht: Reidel), 39
Schmutz, W., Leitherer, C., & Gruenwald, R. 1992, PASP, 104, 1164
Schmutz, W., Vogel, M., Hamann, W.-R., & Wessolowski, U. 1993, A&AS, in preparation
Silk, J. 1986, in IAU Symp. 116, Luminous Stars and Associations in Galaxies, ed. C. W. H. de Loore, A. J. Willis, & P. Laskarides (Dordrecht: Reidel), 301
Sparks, B. 1991, FOC Instr. Sci. Rep. FOC 91-053
Spite, M., & Spite, F. 1991, in IAU Symp. 148, The Magellanic Clouds, ed. R. Haynes & D. Milne (Dordrecht: Kluwer), 372
Stetson, P. B. 1987, PASP, 99, 191
Terlevich, E., Diaz, A. I., Pastoriza, M. G., Terlevich, R., & Dottori, H. 1990, MNRAS, 242, 48P
van den Bos, W. H. 1928, Bull. Astron. Inst. Netherlands, 4, 261
Viallefond, F. 1986, in Star-Forming Dwarf Galaxies, ed. D. Kunth, T. X. Thuan, & J. T. Traw Van (Paris: Editions Frontières), 207
Walborn, N. R. 1973, ApJ, 179, 517
———. 1982, ApJ, 254, L15
———. 1984, IAU Symp. 108, Structure and Evolution of the Magellanic Clouds, ed. S. van der Bergh & K. S. de Boer (Dordrecht: Reidel), 243
———. 1986, IAU Symp. 116, Luminous Stars and Associations in Galaxies, ed. C. W. H. de Loore, A. J. Willis, & P. Laskarides (Dordrecht: Reidel), 185
———. 1991, Proc. Massive Stars in Outburst Meeting, ed. C. Leitherer, N. R. Walborn, T. M. Heckman, & C. A. Norman (Cambridge: Cambridge Univ. Press), 145
Walborn, N. R., Ebbels, D. C., Parker, J. W., Nichols-Bohlin, J., & White, R. L. 1992, ApJ, 393, L13
Wampler, E. J., Wang, L., Baade, D., Banse, K., D'Odorico, S., Gouiffes, C., & Tarenghi, M. 1990, ApJ, 362, L13
Wang, Q., & Helfand, D. J. 1991, ApJ, 370, 541
Weigelt, G., et al. 1991, ApJ, 378, L21
Weigelt, G., & Baier, G. 1985, A&A, 150, L18
Worley, C. E. 1984, ApJ, 278, L109